Correction of Polarimetric Radar Reflectivity Measurements and Rainfall Estimates for Apparent Vertical Profile in Stratiform Rain

JOHN KALOGIROS,* MARIOS N. ANAGNOSTOU,*,+ EMMANOUIL N. ANAGNOSTOU,# MARIO MONTOPOLI,@,& ERRICO PICCIOTTI,& AND FRANK S. MARZANO+,&

* *Institute of Environmental Research and Sustainable Development, National Observatory of Athens, Athens, Greece*
+ *Department of Information Engineering, Sapienza University of Rome, Rome, Italy*
# *Department of Civil and Environmental Engineering, University of Connecticut, Storrs, Connecticut*
@ *Department of Geography, University of Cambridge, Cambridge, United Kingdom*
& *CETEMPS Centre of Excellence, University of L'Aquila, L'Aquila, Italy*

(Manuscript received 30 May 2012, in final form 29 November 2012)

ABSTRACT

A method for correcting the vertical profile of reflectivity measurements and rainfall estimates (VPR) in plan position indicator (PPI) scans of polarimetric weather radars in the melting layer and the snow layer during stratiform rain is presented. The method for the detection of the boundaries of the melting layer is based on the well-established characteristic of local minimum of copolar correlation coefficient in the melting layer. This method is applied to PPI scans instead of a beam-by-beam basis with the addition of new acceptance criteria adapted to the radar used in this study. An apparent vertical profile of reflectivity measurements, or rainfall estimate, is calculated by averaging the range profiles from all of the available azimuth directions in each PPI scan. The height of each profile is properly scaled with melting-layer boundaries, and the reflectivity, or rainfall estimate, is normalized with respect to its value at the lower boundary of the melting layer. This approach allows variations of the melting-layer boundaries in space and time and variations of the shape of the apparent VPR in time. The application of the VPR correction to reflectivity and rainfall estimates from a reflectivity–rainfall algorithm and a polarimetric algorithm showed that this VPR correction method effectively removes the bias that is due to the brightband effect in PPI scans. It performs also satisfactorily in the snow region, removing the decrease of the observed VPR with range but with an overestimation by 2 dB or more. This method does not require a tuning using climatological data, and it can be applied on any algorithm for rainfall estimation.

1. Introduction

The deployment of weather radars in mountainous terrain introduces problems such as the partial or complete beam blockage of the radar beam and ground clutter at low elevation angles of the radar antenna. For quantitative precipitation estimation in complex terrain, radar measurements are taken at higher-elevation scans to avoid these problems. This observational geometry in combination with low heights of the freezing level during widespread (stratiform) precipitation causes the radar resolution volume to be located often within the melting layer or snow regions, causing significant biases in the surface rainfall estimates (Smith 1986). Such a problem may also occur in long-range observations of operational radars even at low elevation angles because of beam broadening and height increase with range. Radar observations in the melting layer are associated with an enhancement of radar reflectivity, a phenomenon called bright band (Battan 1973). The primary causes of this reflectivity enhancement are the rapid increase of the dielectric constant (due to melting snow) and the change of the shape of hydrometeors at the top of the melting layer followed by an increase of the fall velocities of hydrometeors at the end of the melting process and reduction of snowflakes to raindrops (Battan 1973; Fabry and Zawadzki 1995). Reflectivity at horizontal polarization is a dominant radar measurement in the estimation of rainfall rate using either a reflectivity–rainfall relation or polarimetric algorithms (Bringi and

Corresponding author address: John Kalogiros, Institute of Environmental Research and Sustainable Development, National Observatory of Athens (NOA), Lofos Koufou, P. Penteli, 15236, Athens, Greece.
E-mail: jkalog@noa.gr

DOI: 10.1175/JAMC-D-12-0140.1

Chandrasekar 2001). Thus, to estimate rainfall rate at ground level, a correction of radar measurements for melting-layer effects is required.

The vertical profile of reflectivity (VPR) is a term used in the literature to describe the vertical variation of the difference between the reflectivity within the melting layer and the snow layer above it and the reflectivity close to the ground. The profile of reflectivity below the melting layer is assumed to have small vertical variations. Smith (1986), based on previous work of Harrold and Kitchingman (1975), presented a method for detection of peaks in reflectivity profiles using plan position indicator (PPI) scans at two different elevation angles. Correction of the reflectivity (i.e., reduction of reflectivity measurements to near ground level) was achieved using a triangular model of VPR in the melting layer and a linear reduction of reflectivity in the snow layer (aggregation of snowflakes while approaching the melting layer). Kitchen et al. (1994) proposed a VPR correction method using an idealized VPR shape estimated from climatological data, surface observations, and infrared satellite data to derive the melting-layer boundaries and an orographic enhancement of reflectivity below the melting layer. Kitchen (1997) improved that method by replacing the climatological values of the parameters of the idealized VPR with values estimated from the best fit of the idealized VPR to reflectivity measurements from scans at various elevation angles. Andrieu and Creutin (1995) proposed a nonlinear inversion method to correct reflectivity for VPR using scans at two different elevation angles similarly with Smith (1986) and the assumption of VPR spatial (horizontal) homogeneity. Vignal et al. (1999) proposed a generalization of the VPR correction of Andrieu and Creutin (1995) using scans at many elevation angles and identifying VPR variations at scales of a couple of tens of kilometers. This correction scheme was further adapted to cases with spatiotemporal variations of VPR and different rain types in space–time-varying areas by Delrieu et al. (2009) and Kirstetter et al. (2010). Gourley and Calvert (2003) described an automated brightband detection method using radar volume data and weather forecast model data, while Bellon et al. (2005) estimated VPR from 30-min averages of reflectivity profiles using near-range constant-altitude angle plan position indicator (CAPPI) radar data. A similar technique was used by Marzano et al. (2004) to reconstruct the vertical profile of reflectivity in beam-occluded areas by using radar data of nonblocked radar gates.

The above VPR correction methods, some of which quite complicated, are characterized by the usage of single-polarization reflectivity measurements at two or more elevation angles, long time integration periods, and auxiliary a priori information on the melting-layer characteristics. Smyth and Illingworth (1998) proposed a polarimetric measurement (the linear depolarization ratio L_{dr}) in addition to reflectivity to detect snow and graupel and then construct median climatological vertical profiles of reflectivity separately for stratiform rain, snow, and graupel showers taking into account beamwidth effects. Rico-Ramirez et al. (2005, 2007) also described a method to classify hydrometeors and detect the melting layer using polarimetric measurements (reflectivity at horizontal polarization, differential reflectivity, and L_{dr}) and then apply a correction using an idealized VPR correction constructed from climatological data. Recently, Matrosov et al. (2007), based on the method of Brandes and Ikeda (2004) that detects the freezing level (0°C isotherm, the top of the melting layer) using polarimetric radar measurements, suggested a VPR correction method for polarimetric radars applied on a beam-by-beam basis. This method uses the copolar correlation coefficient ρ_{hv} to automatically identify the boundaries of the melting layer, which are, thus, allowed to vary in time and space. The copolar correlation coefficient in the melting layer presents a characteristic local minimum because of the mixture of different types of hydrometeors (Bringi and Chandrasekar 2001), whereas the detection of the melting layer from reflectivity measurements may fail because of spatial variations and discontinuities of the bright band and the smoothing effect of the radar volume (beam broadening). The local minimum of ρ_{hv} in the melting layer may not be as clear as the increase of L_{dr} (Illingworth and Thompson 2011), but unlike reflectivities and L_{dr}, ρ_{hv} is not affected by path attenuation, which is significant for high-frequency radars (like X band). After the detection of the melting-layer boundaries an idealized VPR shape is used similar to Smith (1986) with predetermined characteristics (like the peak value in melting layer and the slope of the profile in the snow layer) derived from available datasets of range–height indicator (RHI) radar cross-section scans and vertically pointing radars. The reduction of the measured VPR peak value with range due to the increase of the smoothing effect of beam broadening with range and the difference of the middle of the melting layer from the height of the peak of reflectivity enhancement, as well as attenuation of the radar signal, were taken into account in the construction of the idealized VPR.

This work presents an extension of Matrosov et al. (2007) method to PPI scans by using the apparent VPR shape with temporally variable characteristics, which are determined from radar data itself. In this respect the method presented here is called an *apparent* VPR correction, while the Matrosov et al. (2007) method is called

an *idealized* VPR correction. The apparent VPR is different from the true VPR because it includes the effects of beam broadening (and the possible nonuniform beam filling) and the slant profile with horizontal averaging of the spatial variations (Andrieu and Creutin 1995). The idealized VPR correction is implemented and used in this work for comparison purposes. The usage of an apparent VPR shape, rather than a predetermined one, is supported by analysis of radar data where we note that the observed VPR shape is usually not of triangular shape in the melting layer, the peak value varies significantly (by a couple of decibels), and the radar volume smoothing of VPR depends on beamwidth (and antenna rotation rate in the case of RHI scans). Accurate estimation of the boundaries of the melting layer is also required for the application of a predetermined VPR, but ρ_{hv} thresholds that are used to estimate the boundaries depend on the radar measurement noise. Finally, it is noted that the method of Matrosov et al. (2007) cannot be applied to polarimetric rainfall estimators. These estimators, in addition to the reflectivity Z_h at horizontal polarization, use the differential reflectivity Z_{dr}, which usually presents a peak in the melting layer (Bringi and Chandrasekar 2001), and the specific differential phase shift K_{dp}. The method presented in this work is applied directly on the rainfall retrievals therefore can be used to correct any radar–rainfall (polarimetric or reflectivity based) algorithm. For this reason the VPR abbreviation in this work has a double meaning of vertical profile of rainfall estimate from polarimetric radar observables and vertical profile of reflectivity. The method is evaluated in this study based on stratiform type precipitation events. Other cases of vertical variability of reflectivity, such as those in shallow warm or deep convective rain clouds, where a continuous decrease of reflectivity with range due to the increase of the beam height may occur, are not considered here.

The paper is organized as follows. The new method for the construction of the apparent VPR is described in section 2 and examples of its application to RHI and PPI scans are presented. In section 3 a case study with results from the application of the proposed method to PPI scans in comparison to disdrometer reflectivity and rainfall data at the ground is presented in detail. The performance of the proposed algorithm is also evaluated against rain gauge data from another rain event in a different area. Conclusions are drawn in section 4.

2. Description of the method

The proposed VPR correction method is applied here to data collected with the mobile dual-polarization and Doppler X-band radar (X-Pol) of the National Observatory of Athens, which has a beamwidth of 1°. X-Pol measures in PPI and RHI scans the reflectivity Z_h and Z_{dr} (both affected by path attenuation), the differential phase shift Φ_{dp} and ρ_{hv}. The estimation of K_{dp} from Φ_{dp} is made using a linear polynomial filtering of 2 km in length and then a numerical gradient operator. The bias calibration of Z_h and Z_{dr} is made using long-term disdrometer data as described in Kalogiros et al. (2013a). The removal of propagation and scattering effects on these polarimetric observables in rain is achieved using the algorithm described by Kalogiros et al. (2013a). Although the quantitative maximum range for an X-band radar is between 60 and 100 km, the VPR correction method developed herein can be applied to longer-range C-band and S-band polarimetric radars as well.

a. Detection of melting-layer boundaries

The melting-layer signature of copolar correlation coefficient (its systematic local minimum) is typically observed in RHI scans with polarimetric radars during stratiform rain events. To estimate the melting-layer thresholds of ρ_{hv} for X-Pol and apply the melting-layer detection method proposed by Matrosov et al. (2007) a large number of RHI scans, acquired with that system since 2007, were analyzed. Matrosov et al. (2007) proposed ρ_{hv} thresholds of 0.95 and 0.90 for the detection of the lower and the upper boundaries of the melting layer, respectively, in slant (low elevation angle) beams. The lower and upper boundaries of the melting layer correspond to the terms *bottom* and *top* height of the melting layer, respectively, used in this work. These boundaries should not be considered as exact limits of the different physical processes taking place in the melting layer and the region above it, but as an approximate estimation of them, which is sufficient for the purpose of VPR correction. For slant beams range r corresponds to height h through the simple geometrical relation $h = r \sin(\theta_{el})$, where θ_{el} is the elevation angle of the antenna using a flat Earth and homogeneous troposphere model, or the height can be derived similarly with geometrical optics by including the effects of atmospheric refraction for a standard atmosphere model and Earth curvature (Doviak and Zrnić 1993), which is a more accurate approach for long-range radars. The choice of Matrosov et al. (2007) for the value of 0.95 of ρ_{hv} for the detection of the bottom of the melting layer was based on their observation from RHI data that ρ_{hv} values in the rain layer below the melting layer were steadily above 0.95. However, the measured rain values of ρ_{hv} in RHI scans of X-Pol were usually above 0.97. If this ρ_{hv} threshold is set high the result is no detection of the decrease from the high threshold value in the rain region to a lower

value in the melting layer. If this ρ_{hv} threshold is set low the result is probably many false detections, most of which should be rejected using the rest of the criteria described in the next paragraph. Thus, this ρ_{hv} threshold must be set to the typical value of ρ_{hv} in rain for the considered radar. In addition, the minimum values of ρ_{hv} in the melting layer were sometimes above 0.90 and ρ_{hv} returned to values a little less than 0.97 in the snow layer. Thus, the value of 0.96 for ρ_{hv} (i.e., a value 0.01 less than the value for the detection of the bottom of the melting layer) was selected for the detection of the top of the melting layer.

Based on the analysis of a large number of RHI scans collected with X-Pol, additional criteria were introduced for the acceptance of melting-layer detection in the radar scans and to exclude possible false detections due to random variations in ρ_{hv} measurements. These criteria require that ρ_{hv} is above 0.97 for 50 m (or at least three points) of the profile below the melting-layer bottom and above 0.96 for 50 m (or at least three points) of the profile above the melting-layer top, while the minimum acceptable depth of the melting-layer depth is 150 m (Fabry and Zawadzki 1995). In the melting layer the minimum ρ_{hv} has to be less than 0.93, and the difference between the peak value of Z_h in the melting layer and the value of Z_h at its bottom has to be more than 1.5 dB. This low value of acceptable reflectivity enhancement in the melting layer is taking into account the smoothing of the reflectivity profile due to beam broadening and, thus, the reduction of observed reflectivity enhancement with range (Matrosov et al. 2007) (as shown in Fig. 5a discussed in section 2b). Possible ground clutter, which appears as a spurious local minimum in the ρ_{hv} profile, is detected and rejected in regions where the minimum ρ_{hv} is less than 0.6. If Doppler measurements are available (as it is the case of X-Pol), ground clutter can be detected in regions where the radial Doppler velocity is less than 1 m s^{-1} and the spectrum width is less than 1 m s^{-1}. These are the maximum expected values (Doviak and Zrnić 1993) for ground clutter from stationary rigid targets, vibrating foliage, etc., and a rotating radar antenna with a rotation rate for X-Pol data up to 6° s^{-1} in PPI scans.

Figure 1 presents a sample RHI scan (3° s^{-1} antenna rotation rate) with melting-layer signature and its boundaries detected with the above ρ_{hv} thresholds and acceptance criteria. It is noted that the reported values of ρ_{hv} thresholds depend on the performance of the radar system and the exact values given here are specific to the X-Pol radar used in this study. The detection was carried out in the vertical direction of a Cartesian grid instead of the polar grid of the radar observations (generally slant beams) after a two-dimensional linear

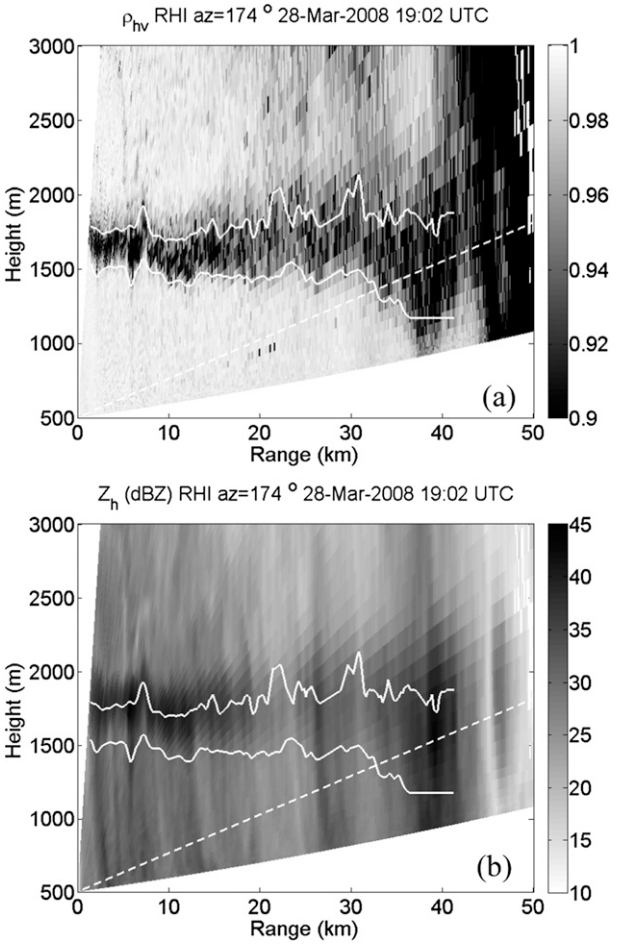

FIG. 1. RHI scan measurements of (a) copolar correlation coefficient ρ_{hv} and (b) horizontal reflectivity Z_h at the azimuth direction (az) of 174° of the disdrometer on 28 Mar 2008. The white solid lines correspond to the detected boundaries of the melting layer. The white dashed line corresponds to a ray with an elevation angle of 1.5°.

interpolation in a grid with a step of 200 m in the horizontal axis (range) and 25 m in the vertical axis (height). At ranges where the melting layer was not detected linear interpolation of melting-layer boundaries was carried out. The radar volume smoothing effect is apparent as beam broadening of the melting-layer depth and a less evident average reduction with range of the difference between the reflectivity maximum in the melting layer and the reflectivity value at its bottom (Ryzhkov 2007). The radar reflectivity Z_h shown in Fig. 1b was corrected for the rain-path attenuation along each radar ray until the bottom of the melting layer using the algorithm of Kalogiros et al. (2013a), which is strictly valid at low elevation angles of the RHI scan (i.e., at range values greater than about 10 km for the melting-layer bottom). The volume smoothing also affects

ρ_{hv} and the melting-layer detection becomes difficult at ranges longer than 40 km, where the melting-layer bottom and low ρ_{hv} values extend down to the minimum measurement altitude of this RHI scan. According to Fig. 1b the maximum values of Z_h are located on average at the upper half of the melting layer, which was also observed by Matrosov et al. (2007). The average height difference between the Z_h peak and the ρ_{hv} minimum in the melting layer (at about the middle of the melting layer) in RHI scans of X-Pol was found to be 65 m, while Matrosov et al. (2007) reported an average height difference of 105 m. The variation of ρ_{hv} values in the melting layer is the result of the variation in the mixture of particle types with the minimum value at the height of balance in the contributions from wet snow and raindrops, whereas the Z_h enhancement is the result of the aggregation and melting-layer processes and the peak generally occurs when large snowflakes melt to form small raindrops (Bringi and Chandrasekar 2001). As snowflakes fall their melting occurs before the balance between wet snow and raindrops is achieved and, thus, the peak of Z_h occurs a little higher than the altitude of minimum ρ_{hv}. Figure 1b also shows typical spatial variations and discontinuities of the bright band combined with similar variations in the rain layer below, which make difficult the melting-layer detection using reflectivity measurements alone.

Figure 2 presents radar measurements from a PPI scan at an antenna elevation angle of 1.5° within 1 min before the RHI scan shown in Fig. 1. Azimuth sectors with missing data are due to blockage by terrain features. The white circle corresponds to the site of the bidimensional-video disdrometer, which was installed together with three rain gauges at a distance of 35 km to the south of the radar and an altitude of 12 m above mean sea level. The azimuth of the installation site of the disdrometer is the azimuth value of the RHI scan in Fig. 1. For the detection of melting-layer range boundaries in PPI scans it was found that the ρ_{hv} thresholds (0.97 and 0.96) that are used in RHI scans gave limited number of detections. Lowering these values by 0.04 (0.93 and 0.92 ρ_{hv} thresholds for the boundaries and requirement for less than 0.89 minimum ρ_{hv} value in the melting layer) the detections were doubled and the estimated depth of the melting layer was closer to the results from corresponding RHI scans (see Fig. 6a). This difference between PPI and RHI scans is probably due to the different scanning geometry (azimuth vs elevation scans) and the different antenna rotation rate (6° vs 3° s^{-1} for PPI and RHI scans, respectively). Thus, each radar ray (dwell), which is the result of the processing of a significant number of radar pulses (104 pulses for the current setup of X-Pol), corresponds to different spatial smoothing.

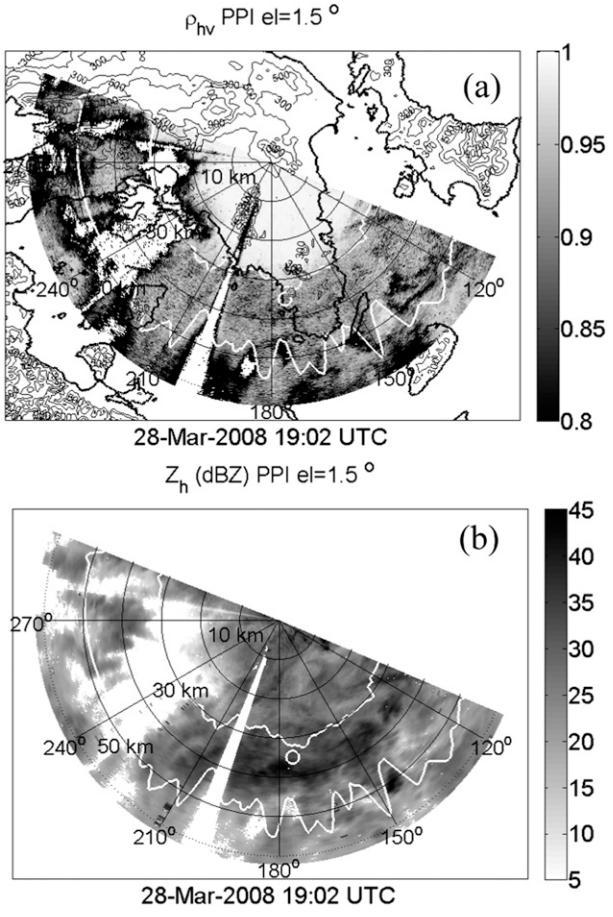

FIG. 2. As in Fig. 1, but for a PPI scan at an antenna elevation angle of 1.5°. The white circle indicates the position of the disdrometer. In (a), terrain elevation above sea level is shown with contours and labels in meters and the coastline is shown with a thick black line.

In PPI scans the horizontal scanning introduces horizontal averaging of spatial variations, which lead to a small decorrelation between the two polarization returns similar with the beam broadening and filling effects described by Ryzhkov (2007). In RHI scans in addition to the smaller rotation rate of the antenna the averaging due to scanning is made in the vertical direction where the decorrelation between the two polarization returns with height is probably smaller. As in the case of RHI scans at ranges where the melting layer was not detected linear interpolation of melting-layer boundaries was carried out. To consider a radar volume scan affected by melting-layer effects, the minimum acceptable percentage of rays with detection of melting layer with respect to the total rays of a PPI scan with signal in the average boundaries of the detected melting layer has to be 40% (i.e., a little lower than the majority of rays, in favor of the acceptance of melting-layer detection). In

this way false detections, for example during convective type rain, are rejected and the VPR correction described in section 2b is not applied. The melting layer appears as an annular feature (near-circular zone) of enhanced reflectivity in the PPI scan of the 1.5° elevation angle in Fig. 2. A moving average of 5 points (an azimuth sector of about 3° for the X-Pol data) was applied to the boundaries of the melting layer, shown in Fig. 2, to smooth out variations due to detection errors especially of the top of the melting layer.

Another difference between the detection of melting layer in RHI and PPI scans is that in single PPI scans it is not possible to interpolate data on a Cartesian grid with a vertical direction and, thus, slant profiles have to be used. The dashed lines (slant rays) in Figs. 1a and 1b correspond to an elevation angle of 1.5°. For that specific time of the RHI scan the slant profile at the elevation angle of 1.5° crosses the bottom of the melting layer at a range of about 30 km, but because of radar volume smoothing it is not possible to estimate from range profile data where the radar beam crosses the top of the melting layer. The detection of the melting layer from the interpolated RHI data on a Cartesian grid as described above is also difficult at that range. In addition, a slant profile may cross horizontal undulations of the melting-layer boundaries (like the undulations observed in Fig. 1), which will appear as erroneous melting layers of small depth in the ρ_{hv} profile. To detect the melting layer in a slant profile from a PPI scan like the one shown in Fig. 1 where the upper boundary cannot be detected using the recovery of ρ_{hv} to the value of 0.92 for 50 m of the profile above the melting layer, the upper boundary is taken as the maximum height where ρ_{hv} value is above 0.92. In conclusion, the detection of melting-layer boundaries (especially its upper boundary at low elevation angles and long ranges) using ρ_{hv} in a PPI scan is quite more challenging than in an RHI scan. If the radar volume scan includes one or more RHI scans, the boundaries of the melting layer detected in these scans can provide some auxiliary information (e.g., the height search limits) for the detection of the melting layer in the PPI scans.

b. Construction of apparent VPR

To apply a VPR correction to radar data from RHI or PPI scans, the VPR has to be determined as an idealized profile with parameters estimated from climatological data or from the real-time radar data. Both approaches have been used in previous methods for estimation of the profile of reflectivity as mentioned in section 1. The usage of real-time radar RHI or PPI scans allows temporal and spatial variations of VPR and, thus, a potential improvement of the VPR correction. Previous methods that used real-time PPI scans required scans at two or more elevation angles with assumptions like that the scan at the lowest elevation angle is not affected by VPR effects or using complex nonlinear inversion methods mentioned in the introduction section. The polarimetric detection method proposed by Matrosov et al. (2007) and its modifications for X-Pol, presented in section 2a, gives the possibility for a much simpler alternative to estimate the VPR in each radar scan. Matrosov et al. (2007) used historical radar data to estimate an idealized VPR, while the melting-layer boundaries were determined with the polarimetric method and were allowed to vary in space and time. The correction method used in this work estimates an average VPR shape for each radar scan using only radar data of that scan. The assumption made here is that in the area of the radar scan the shape of the VPR does not vary significantly during the scan duration, while the melting-layer boundaries may vary. For a PPI scan at a 1.5° elevation angle of the antenna, a 100-m variation of the melting-layer bottom height in the scan corresponds to a 3.8-km range variation, which gives a small change (0.2 dB) of the peak of Z_h VPR because of volume smoothing according to Matrosov et al. (2007). Thus, the peak value of the VPR may be assumed to be constant in the PPI scan, but a 100-m variation of the melting-layer bottom is significant with respect to its depth (a couple of hundred meters). Melting-layer boundaries (and especially the bottom boundary) may present significant variations in the scan area, especially in mountainous terrain areas. As already mentioned, the new aspect introduced in the proposed method, in addition to its application to PPI scans, relative to Matrosov et al. (2007) correction method is that it does not use an idealized VPR shape (triangular shape with predetermined peak value in the melting layer and a predetermined linear trend in the snow layer above), but the shape of the VPR is estimated by the scan data.

Figure 3 presents the block diagram of the algorithm for melting-layer detection and VPR correction, where the variable P may be Z_h or Z_{dr} in linear units or the estimated rainfall rate R. These parameters are characterized by a profile with a peak in the melting layer (Bringi and Chandrasekar 2001) and a near-exponential negative trend above it, according to the observations. The K_{dp} may not present such a clear signature in and above the melting layer. The average shape of VPR in a scan area is constructed after the detection of melting-layer boundaries, as described in detail in section 2a. The main points of the algorithm steps for detection of melting-layer boundaries and validation of the melting layer are summarized in Fig. 3. The detection is based on predefined threshold values of copolar correlation

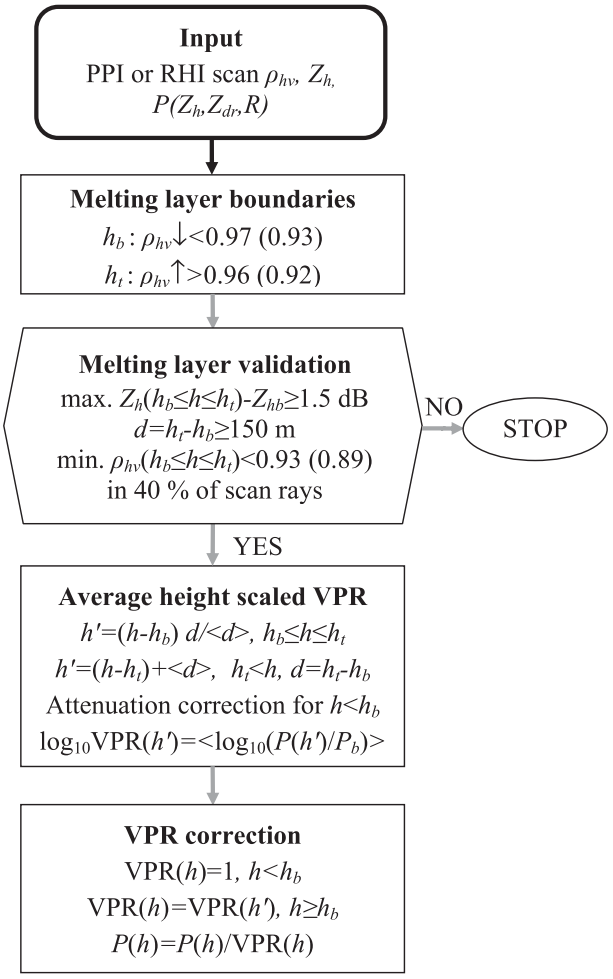

FIG. 3. Block diagram of the VPR correction algorithm. The radar measurement height is indicated by h, and the radar parameter (Z_h or Z_{dr} in linear units or the estimated rainfall rate R) to be corrected is indicated by P. The subscripts b and t indicate a value at the bottom and top, respectively, of the melting layer. The angle-bracket operator indicates scan average. Values of ρ_{hv} thresholds in parentheses are for PPI scans; otherwise the values are for RHI scans. Down and up arrows indicate that ρ_{hv} stays higher than the indicated limit value for at least 50 m of height (minimum of three data points) below or above the corresponding boundary, respectively.

coefficient ρ_{hv}, and the validation of the detection is mainly based on threshold values for the difference of the peak of Z_h in the melting layer from its value Z_{hb} at its lower boundary, the melting-layer depth $d = h_t - h_b$ (h_b is the bottom and h_t is the top height of the melting layer), and the minimum value of ρ_{hv} in the melting layer. Valid detections should include 40% of the total rays of the scan with signal in the average boundaries of the detected melting layer to continue to the rest steps. As mentioned in section 2a, this criterion aims to reject false detections when the convective type of rain dominates over stratiform rain. The complex detection of space–time-varying areas with different type of rain (stratiform or convective) and, thus, different VPR as it is described by Delrieu et al. (2009) and Kirstetter et al. (2010) requires full volume data from many elevation angles and nearly stationary conditions in a time period of 1 h instead of single PPI scans used here. The method presented here does not consider convective rain and applies only to stratiform rain. In convective rain, a reflectivity enhancement and a characteristic minimum of ρ_{hv} similar to the melting layer is not observed. An extension of the current method could be the application of different VPR corrections to the rays where melting layer was detected (stratiform rain) and the rays where it was not detected (possibly nonstratiform rain). However, this was tested and for the moment it is found to cause significant errors and discontinuities between rays because of possible detection errors. The addition of more polarimetric parameters, like the linear depolarization ratio if it is available, would be useful for a more accurate detection of the melting layer.

The construction of the average apparent VPR in the scan is made by averaging the logarithm of the ratio of P values to the corresponding value P_b at the bottom of the melting layer. The logarithmic average, which is equivalent to geometric mean, has the advantage of giving small weight to outlier values relative to the usual average. Spatial variations of the shape of VPR in the radar scan are considered as a spatial random noise that is removed by the averaging. Radar parameters Z_h and Z_{dr} are first corrected for rain-path attenuation below the melting layer using the algorithm of Kalogiros et al. (2013a). The bottom boundary of the melting layer is detected with the method described in section 2a using ρ_{hv}, which is not affected by the path attenuation. Above the melting-layer bottom it is assumed that the attenuation of radar signal is accounted for on average in the estimated VPR similarly to Matrosov et al. (2007). Only signal data, which are determined as the data with signal power above the noise level of about -110 dBm for the herein X-Pol system and ρ_{hv} greater than 0.6, from the rays where melting layer has been detected are used in the averaging for the construction of the apparent VPR. Because the melting-layer boundaries may vary in the scan the averaging is performed in gate bins of a scaled height h' with a gate length of 10% the average depth $\langle d \rangle$ of the melting layer in the scan (the angle-bracket operator indicates scan average). The scaled height h' in the melting layer is estimated from the difference between the measurement height value h and the local h_b height scaled with the ratio of the local depth of the melting layer d to the average depth. Above the melting-layer top, h' is estimated as the

addition of the average depth $\langle d \rangle$ with the difference between h and h_t. In this way the continuity of h' at the melting-layer top is satisfied. This scaling of height is indicated by the expected idealized VPR and allows the melting-layer boundaries to vary within the radar scan. The shape of the apparent VPR with height scaling should depend on the physical processes (i.e., on the large-scale weather system) that occur in the melting layer and the snow layer above it and, thus, it is expected to be the same in a rather extended region around the radar. The VPR above the height of the first positive gradient (presumably due to spatial variations effects) in the snow layer is set to a constant value, because the VPR is expected not to increase with height in this region as a result of aggregation of the falling snowflakes. The height that this may occur is typically well above (500 m or more; see the decreasing gradient with height in Fig. 4) the melting layer. Thus, there is a decorrelation between the rainfall estimates at these altitudes with the rainfall field at the ground, which causes the observed VPR to be unrelated to the physical processes that occur in the snow layer. The use of a constant value for the VPR at these altitudes probably adds no more bias to measurements.

In the final step of the algorithm, the VPR correction is applied to each data point above the melting-layer bottom by using the VPR value at the scaled height that corresponds to the measurement height. Figure 4 presents examples of average scaled profiles of Z_h VPR for the RHI (using data in the range 0–30 km) and PPI scans of Figs. 1 and 2. The average scaled profile shown in Fig. 4b is not the true VPR, but the apparent VPR. The apparent VPR is sufficient for the correction of the scan from which it is estimated. If the true VPR could be estimated (as is done by inversion methods described in the introduction section), then an apparent VPR for each PPI scan in the volume scan could be estimated to correct that scan, which introduces many uncertainties. Thus, it is not surprising that the apparent VPR shapes for RHI and PPI scans are not similar even though they are very close in time. The exact knowledge of the boundaries of the melting layer is also not critical, because no idealized profile has to be applied for the VPR correction of the scan data but the VPR shape is estimated by the data of the same scan. The idealized profile shown in Fig. 4a is the one proposed by Matrosov et al. (2007), but with a 65-m height difference between the peak Z_h VPR and the minimum of ρ_{hv} in the melting layer instead of 105 m used in Matrosov et al. (2007), as already mentioned in section 2a, and using the peak value proposed in that paper at the range of 15 km (the average of ranges from 0 to 30 km). It is clear that the differences between the idealized VPR and the apparent RHI VPR can be a couple of dB, which is significant.

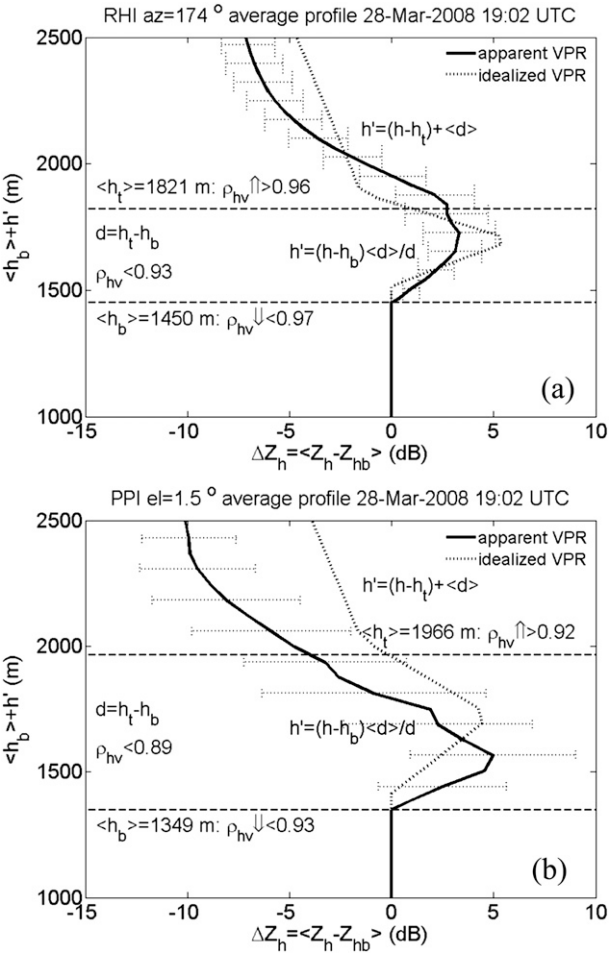

FIG. 4. Scaled apparent VPR of horizontal reflectivity difference ΔZ_h for (a) the RHI scan in Fig. 1b (average from ranges 0 to 30 km) and (b) the PPI scan (average from all available azimuth directions) in Fig. 2b. Horizontal bars correspond to standard deviation. The idealized VPR according to Matrosov et al. (2007) is also shown.

The difference of the idealized VPR from the apparent VPR from the PPI at the 1.5° elevation angle of the antenna in Fig. 4b is even larger and the heights of the peaks of the two profiles do not coincide.

Figure 5 presents statistical results from the detection of melting layer in RHI scans during the rain event of 28 March 2008. The Z_h VPR is estimated as the average difference (or ratio if linear units are used) $\Delta Z_h = Z_h - Z_{hb}$ of horizontal reflectivity Z_h (dBZ) at each height from the horizontal reflectivity Z_{hb} at the bottom of the melting layer. The volume smoothing (beam broadening) effect with range on the peak ΔZ_h value is much larger (more than double) than the reduction of 0.05 dB km^{-1} of the peak value with range reported by Matrosov et al. (2007) for an X-band radar with similar beamwidth to X-Pol. The value of the peak ΔZ_h at

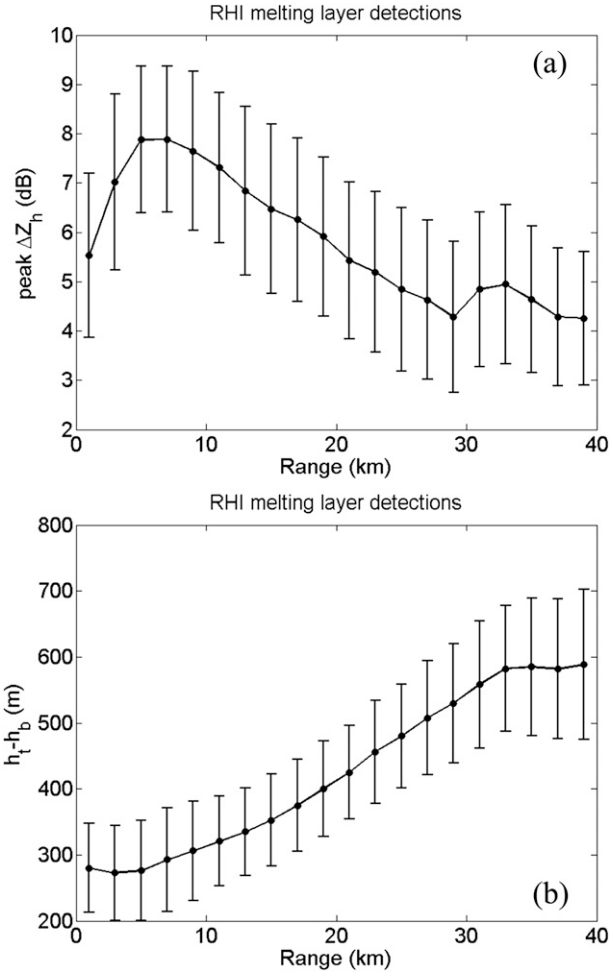

FIG. 5. Average (a) peak ΔZ_h value of the apparent VPR of horizontal reflectivity and (b) melting-layer depth $h_t - h_b$ from RHI scans against range during the rain event of 28 Mar 2008. Vertical bars correspond to standard deviation.

ranges from 5 to 10 km is close to 8 dB, whereas Matrosov et al. (2007) reported a value of 6.8 dB at small ranges and Fabry and Zawadzki (1995) indicated a value between 7.6 and 9.6 dB. It should be noted that the volume smoothing of VPR in the vertical direction depends also on the rotation rate of the radar antenna in the case of an RHI scan, because each radar ray is constructed by averaging a number of pulses as mentioned in section 2a, and that ΔZ_h may depend on the reflectivity Z_{hb} at the bottom of the melting layer (Matrosov et al. 2007). The increase of depth of the melting layer with range from about 300 to 600 m is also due to beam broadening. At ranges greater than 30 km the detection of the melting-layer boundaries is not clear in the RHI scans and the estimated melting-layer depth and peak values tend to a constant value. At ranges closer than about 7 km the peak value of ΔZ_h in melting layer estimated from the RHI scans presents a reduction, while the melting-layer depth tends to a constant value. This reduction is due to the smoothing effect of gate averaging along the radar ray (the gate length was 150 m for this X-Pol data), which dominates the effect of beam broadening at high-elevation angles.

Figure 6 presents common (same range and azimuth) and near-concurrent (within the ~3-min time duration of a full volume scan) melting-layer detection results from PPI and RHI scans on the same rain event as in Fig. 5. With the chosen ρ_{hv} thresholds for PPI scans (section 2a) the detected bottom and upper heights of the melting layer in RHI and PPI scans are quite close. However, the top of the melting layer in ρ_{hv}-PPI scans at low elevation angles like 1.5° (at a range of about 50 km for that rain event) is not clear enough (5-km range variations correspond to 130-m height variations) as it was also mentioned in section 2a (Fig. 2) and its detection presents significantly more variations compared to the detections from RHI scans. According to the results from spatial interpolation of three radiosondes observations in the area of Greece at 1200 and 0000 UTC 28 March 2008 (not shown here) the freezing level varied from 1800 to 2000 m, which agrees on average with the top of the melting layer (the height of return of ρ_{hv} to high values) shown in Fig. 6a. The peak ΔZ_h values used for the construction of the histogram in Fig. 6b are from the slant apparent VPR (scan average scaled profile) in the case of PPI scans, while in the case of RHI scans the peak ΔZ_h values are from the vertical VPR at one azimuth (174°) and one range (the range of the melting-layer bottom in the PPI scan). The range and frequency of peak ΔZ_h values are similar for RHI and PPI scans (i.e., same average and standard deviation values), but the temporal correlation between RHI and PPI peak ΔZ_h values (not shown here) is small. This result suggests that significant differences exist between the slant-apparent VPR in the case of PPI scans and the vertical VPR in the case of RHI scans, which does not include horizontal averaging of spatial variations.

3. Results

a. Case study

This section presents the results from the application of the VPR correction method to a stratiform rain event (28 March 2008) during operation of X-Pol in the north suburbs of Athens (Greece) at an altitude of 500 m above mean sea level. This event was selected because the distance of the disdrometer from the radar was in

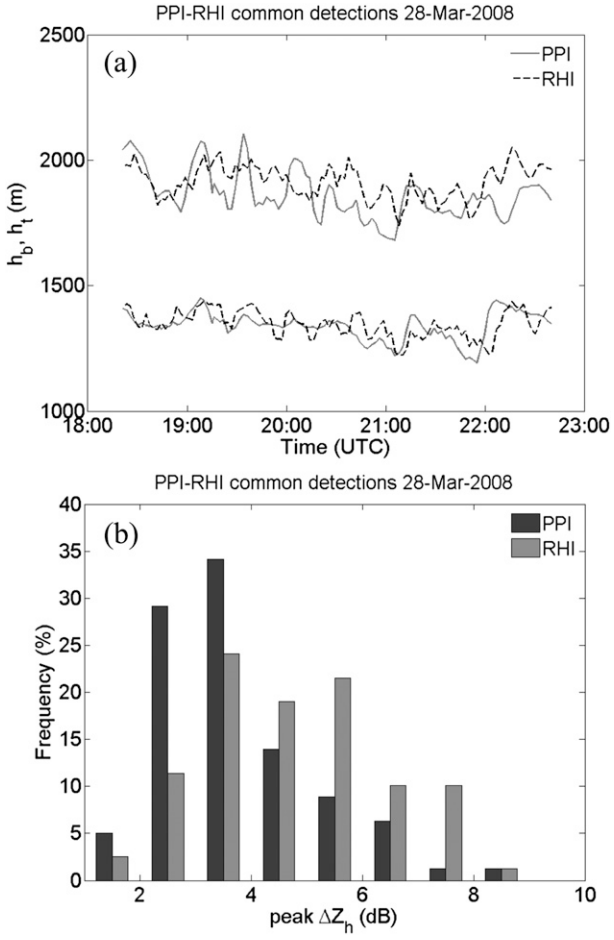

FIG. 6. (a) Time series of melting-layer boundaries bottom (h_b) and top (h_t) and (b) histogram of peak ΔZ_h value of the apparent VPR of horizontal reflectivity from PPI and RHI scans during the rain event of 28 Mar 2008. Common detections were the detections in the same azimuth direction and range and with a temporal separation up to the time duration of a full volume scan (about 3 min).

the melting-layer range boundaries as detected in the 1.5° elevation angle PPI scans. Thus, it was possible to evaluate the VPR correction of the reflectivity Z_h using the reflectivity calculated from the disdrometer data and T-matrix scattering routines (Mishchenko 2000). The evaluation of the VPR correction method using rainfall rate estimates from radar measurements against rain measurements from the disdrometer or rain gauges is affected by the inherent parameterization error in radar rainfall estimates. Thus, validation of the VPR correction method using reflectivity is a more straightforward approach. Moreover, the PPI scan at the 0.5° elevation angle was not affected by the melting layer and, thus, it provided an additional comparison reference for the corrected data from the PPI at the 1.5° elevation angle.

Figure 7 presents the results of the application of the VPR correction method in the same PPI scan (1.5° antenna elevation angle) as in Fig. 2 in comparison with the PPI scan at the 0.5° elevation angle within 1 min before the higher-elevation PPI scan. Even though the rain event is characterized as stratiform (widespread precipitation) there is significant spatial inhomogeneity, which constitutes a challenge for the VPR correction method. Comparing Fig. 2b and Figs. 7a and 7b it can be noted that the brightband zone within the detected boundaries of the melting layer has been significantly reduced, but at the same time the cells of intensive rain are similar between the PPI at 0.5° elevation angle and the corrected PPI at 1.5° elevation angle. More quantitative observations can be inferred from Fig. 7c, which shows that on average in the PPI scans the profile of reflectivity at the 1.5° elevation angle corrected with the apparent VPR is within 2 dB from the reference profile of reflectivity at the 0.5° elevation angle. The corrected profile in the snow region seems to be overestimated in this example, while in the melting layer the difference from the reference profile is within 1 dB. The idealized VPR correction is not so effective and, thus, it requires more adjustments than the change of the height difference between the peak of reflectivity and the middle of the melting layer from 105 to 65 m compared to the mean VPR described by Matrosov et al. (2007). Adjustment of all the parameters of the idealized VPR (such as the peak ΔZ_h value and its range dependence due to volume smoothing and the snow-region reflectivity gradient) for each radar and experimental setting is proposed by Matrosov et al. (2007), but the idealized (triangular) shape of the VPR is probably the critical factor for the reduced performance of that correction (see Fig. 4b).

Figure 8 presents time series of measured and corrected X-Pol Z_h at the range and azimuth of the disdrometer versus Z_h calculated from the disdrometer measurements. The position of the disdrometer (see Figs. 2 and 7) is in the lower half of the melting layer during this rain event. In the first half time period of the event, when the melting-layer effects are more significant in the Z_h measurements from the 1.5° elevation angle PPI scans (as indicated from the comparison with the reference disdrometer and the 0.5° elevation angle radar data), the apparent VPR correction is clearly closer to the reference data (especially the radar data from the 0.5° elevation angle) than the idealized VPR correction. According to Fig. 6a the bottom of the melting layer does not change significantly with time (it has a small negative trend) and, thus, according to the idealized VPR model the VPR correction should not change significantly with time. For this reason the idealized correction

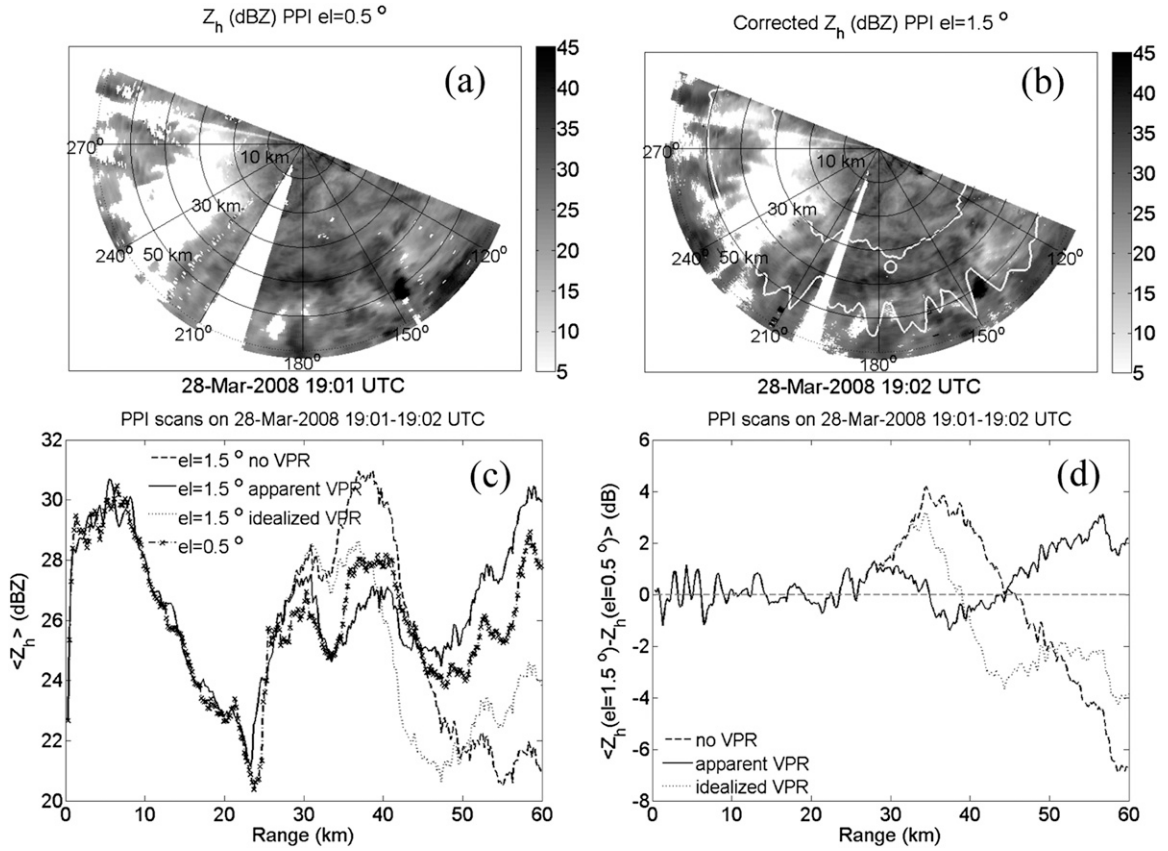

FIG. 7. (a) Horizontal reflectivity Z_h in the PPI scan just before the PPI scan of Fig. 2b but at an antenna elevation angle of 0.5°, (b) Z_h in the PPI scan as in Fig. 2b at an antenna elevation angle of 1.5° but corrected for apparent VPR, (c) the average range profiles of Z_h in the above PPI scans, and (d) the difference of these scan average Z_h profiles at the antenna elevation angle of 1.5° from the profile at 0.5° elevation angle.

underestimates the VPR correction during the first half time period, while the apparent VPR correction follows very well the actual VPR enhancement of Z_h.

Figure 9 presents time series of accumulated rainfall estimates from the radar measurements at the disdrometer range and azimuth using two radar–rainfall algorithms and the average accumulated rainfall measured by the disdrometer and the adjacent rain gauges. The X-band reflectivity–rainfall algorithm is given by the relation

$$R(Z_h) = 3.36 \times 10^{-2} Z_h^{0.58}, \qquad (1)$$

where the units of rainfall rate R are millimeters per hour and Z_h units are millimeters to the sixth power per meter cubed (linear reflectivity) instead of the usual logarithmic units (dBZ). The coefficients of this algorithm were determined from long-term X-Pol observations (in 2005 and 2006) in the area of Athens by Kalogiros et al. (2006) and tested in other radar datasets by Anagnostou et al. (2009 and 2010). The polarimetric algorithm $R(Z_h, Z_{dr}, K_{dp})$ used in this work was developed from T-matrix scattering simulations at X-band by Kalogiros et al. (2013b) for a wide range of rain parameters, and it was based on relations valid at the theoretical Rayleigh scattering limit. This algorithm is given by the relation

$$R_p(Z_h, Z_{dr}, K_{dp}) = 0.8106 F_R(\mu) N_w D_0^{4.67} f_{R2}(D_0), \qquad (2)$$

where the median volume diameter D_0 (mm), the intercept parameter N_w (mm^{-1} m^{-3}), and the shape parameter μ (no units) of the rain drop size distribution are estimated from the polarimetric radar measurements Z_h, Z_{dr}, and K_{dp}. The function $F_R(\mu)$ is

$$F_R(\mu) = (0.6 \times 10^{-3})\pi \times 3.78 \frac{6}{3.67^4} \frac{(3.67+\mu)^{\mu+4}}{\Gamma(\mu+4)} \times \Gamma(\mu+4.67)/(\mu+3.67)^{\mu+4.67}, \qquad (3)$$

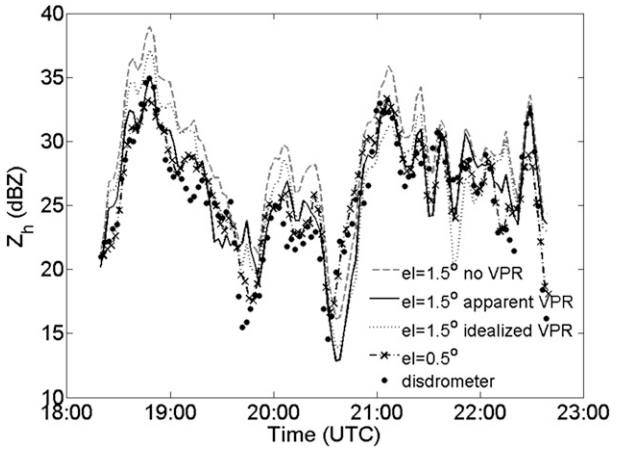

FIG. 8. Time series of measured and corrected for apparent or idealized VPR horizontal reflectivity Z_h from the radar at the range and azimuth of the disdrometer and the disdrometer during the rain event of 28 Mar 2008.

where Γ indicates the gamma function. The third-degree rational polynomial function $f_{R2}(D_0)$ and the estimation of D_0, Nw, and μ from the polarimetric radar measurements are described in detail by Kalogiros et al. (2013b). Equation (2) is a straightforward derivation from the definition of rainfall rate with the addition of function $f_{R2}(D_0)$ to account for an exponential law that was used, instead of a power law for the terminal velocity of raindrops against their diameter (Bringi and Chandrasekar 2001). This polarimetric algorithm was validated against other polarimetric algorithms by Anagnostou et al. (2013).

The apparent VPR correction of radar data from PPI scans at the 1.5° elevation angle in Fig. 9 gives accumulated rainfall very close to the values from the 0.5°-elevation-angle radar data. The idealized VPR correction, which is possible only for the reflectivity–rainfall algorithm, overestimates rainfall (i.e., underestimates the VPR correction) in agreement with Fig. 8. The reflectivity–rainfall algorithm in this rain event underestimates rainfall compared to the disdrometer–rain gauge measurements, while the polarimetric algorithm gives better results. The apparent VPR correction can be applied generally to the rainfall rate in addition to reflectivity. Figure 10 presents PPI maps at the 1.5° elevation angle of the total accumulated rainfall in the event using the two rainfall algorithms with and without the apparent VPR correction. The reflectivity–rainfall algorithm underestimates rainfall with respect to the polarimetric algorithm in the entire PPI area. The VPR correction removes the near-circular zone of enhanced rainfall estimate in the melting layer from 30- to 50-km range, which is evident in the azimuth sector from 100°

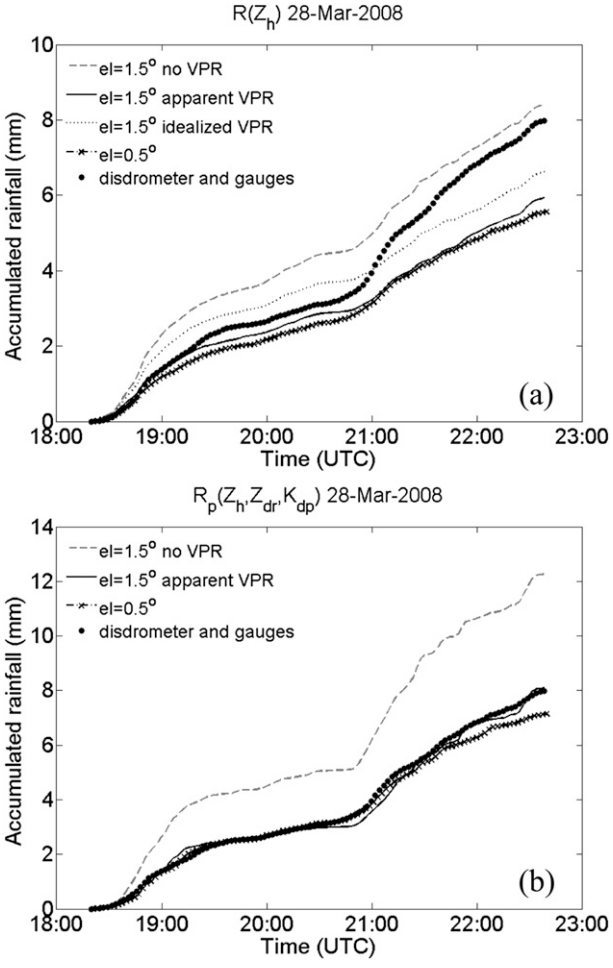

FIG. 9. Time series of accumulated rainfall estimated from the radar measurements with and without VPR correction using (a) the algorithm of Eq. (1) and (b) the polarimetric algorithm of Eq. (2) at the range and azimuth of the disdrometer and the disdrometer during the rain event of 28 Mar 2008.

to 180°. The VPR correction in the snow region possibly gives an overcorrection in the azimuth sector from 210° to 270° at ranges greater than 50 km especially for the polarimetric algorithm. The total accumulated rainfall for the PPI at the 0.5° elevation angle (not shown here) does not present these high rainfall values in the snow region, but it should be noted that at 50-km range the radar beam is quite wide (about 900 m) and its center for the 1.5° elevation angle is located at an altitude of about 1800 m. Thus, the radar beam at the 1.5° elevation angle includes in its lower half the melting layer (its boundaries are shown in Fig. 6a), while the radar beam at the 0.5° elevation angle is still below the melting layer.

Figure 11 presents the difference of average (for the entire rain event) range profiles of Z_h and total accumulated rainfall retrieved from the polarimetric algorithm between the PPI scans at 1.5° and 0.5° elevation angles.

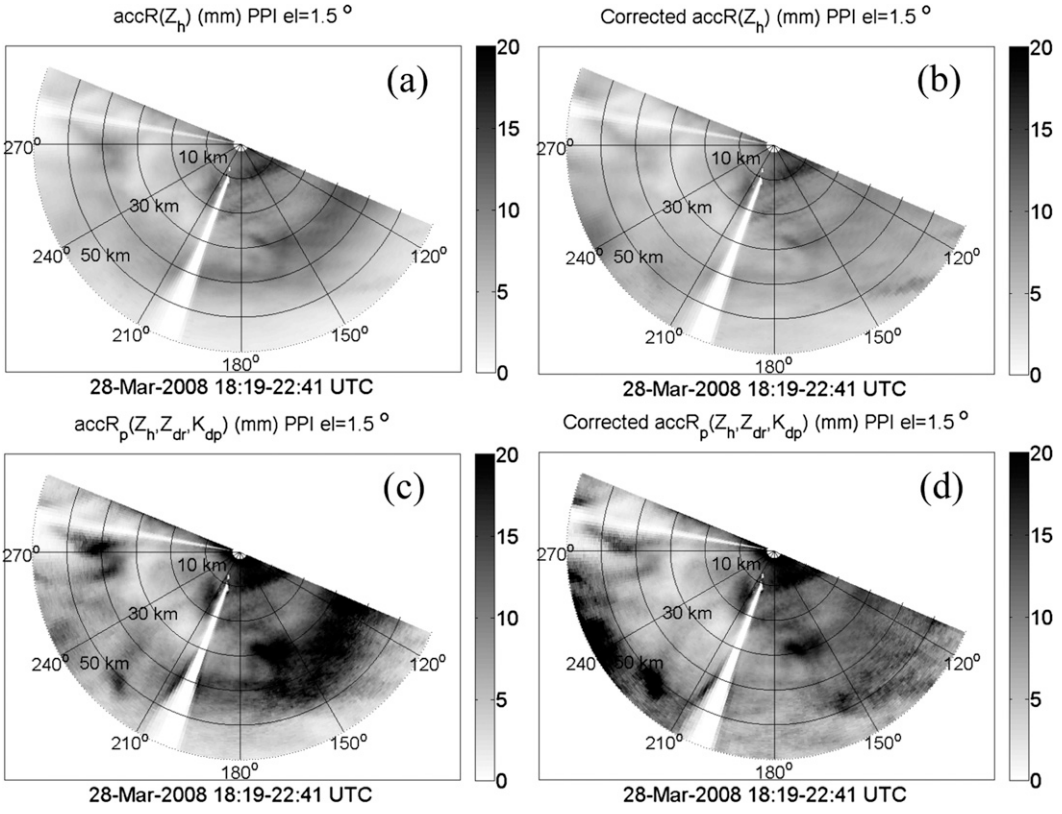

FIG. 10. PPI maps at the antenna elevation angle of 1.5° of total accumulated rainfall estimated from the radar measurements using the algorithm of Eq. (1) (accR) (a) without and (b) with VPR correction and the total accumulated rainfall estimated from the polarimetric algorithm of Eq. (2) (accR$_p$) (c) without and (d) with VPR correction for the rain event of 28 Mar 2008.

The effects of the melting layer and snow region are evident in the raw data of the 1.5° elevation angle. The apparent VPR correction removes these effects leaving no obvious trend with range (i.e., altitude), but the idealized VPR correction does not remove well the enhancement at the lower half of the melting layer and underestimates the correction in the snow region. In the case of the accumulated rainfall (Fig. 11b) the apparent VPR correction does not show any general trend with range, but it makes a moderate overestimation (bias) in both the melting layer and the snow region. The overestimation in the snow region of the range profile is probably due to the overcorrection in the azimuth sector from 210° to 270° at ranges greater than 50 km, which was observed for the VPR correction of the polarimetric algorithm in Fig. 10b.

b. *Evaluation of the algorithm performance against rain gauges*

In addition to the rain event analyzed in the previous subsection data collected with X-Pol in a different geographical area during a field experiment in 2007 (Anagnostou et al. 2009) are used to further evaluate the performance of the apparent VPR correction algorithm described in the present work. During that experimental X-Pol was operating at the northwest part of the island of Crete, near the city of Chania, at an altitude of 177 m above mean sea level. Rain gauges were installed in pairs at various sites within 40-km range from the radar. The terrain of the area was quite complex with a mountainous range (maximum elevation of 2450 m above mean sea level) in the direction east–west within a distance of 20 km to the south of the radar. Therefore, PPI scans were made at high elevation angles (3° and 4°) of the antenna to avoid beam blockage. A rain event with melting-layer signature in the radar scans, many cells of intensive rain, time duration of one day, and high total accumulated rainfall (90 to 150 mm depending on location) was recorded on 22 March 2007. According to the detection of melting-layer boundaries in PPI scans and verified by RHI scans (not shown here) the bottom of the melting layer was quite high (values between 1500 and 2500 m) with significant spatial variations of about

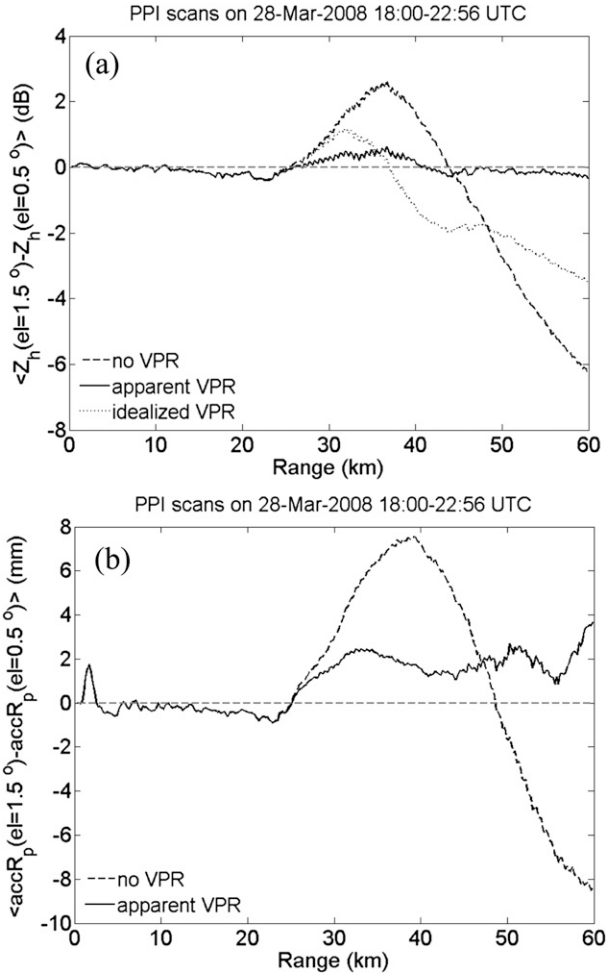

FIG. 11. Scan average difference of range profiles of (a) Z_h and (b) total accumulated rainfall (accRp) estimated using the polarimetric algorithm of Eq. (2) from PPI scans at the antenna elevation angle of 1.5° from the corresponding profiles at 0.5° elevation angle for the rain event of 28 Mar 2008.

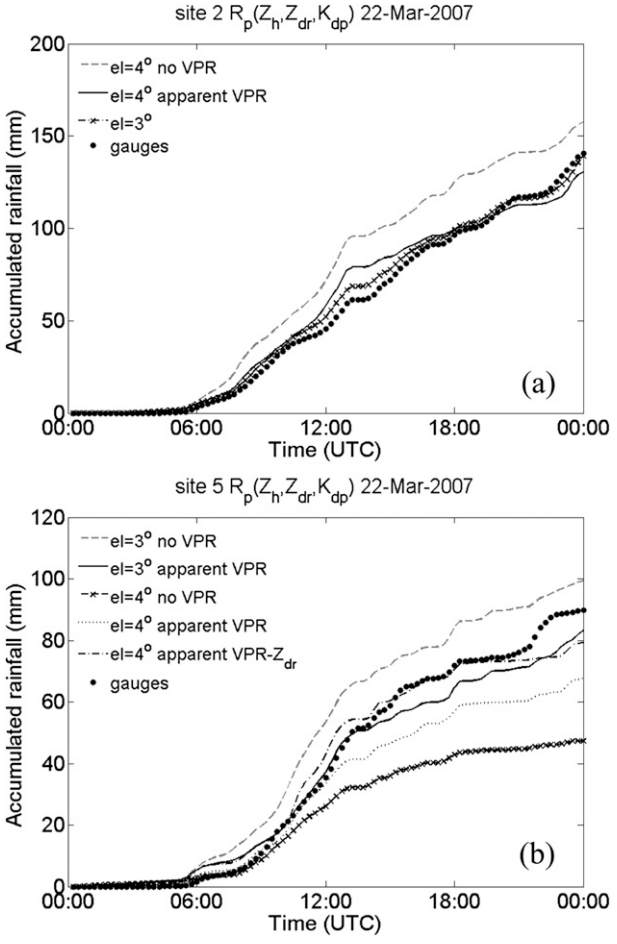

FIG. 12. Time series of accumulated rainfall estimated from the radar measurements with and without correction for apparent VPR of rainfall estimate using the polarimetric algorithm of Eq. (2) (a) at site 2 and (b) at site 5 during the rain event of 22 Mar 2007. In the VPR–Z_{dr} method, Z_{dr} has been corrected first for its apparent vertical profile before correction for VPR of rainfall estimate.

400 m (lower values were detected in the area of the mountainous range), as well a slow increase with time (about 400 m in 12 h). At the last 4 h of the day the bottom of the melting layer decreased rapidly down to 1000 m. This temporal variation of melting-layer bottom corresponds to the passage of a warm front followed by a cold front in a weather depression, which is typical situation during spring time in Greece. Because of the generally high altitude of the bottom of the melting layer only two measurement sites were within and above the melting-layer range boundaries as detected in PPI scans. These two sites were site 2 with an elevation of 1041 m at a range of 25 km from the radar and site 5 with an elevation of 435 m at a range 37 km from the radar.

Figure 12 shows the time series of accumulated rainfall during the day as measured by the rain gauges at the above two sites and estimated from the polarimetric algorithm Eq. (2) with and without correction for apparent VPR. The radar measurements at the elevation angle of the antenna of 3° at the ranges of site 2 and site 5 correspond to an altitude below the melting layer and within the melting layer, respectively. For the elevation angle of the antenna of 4° these ranges of sites 2 and 5 correspond to an altitude in the melting layer and above it in the snow region, respectively. For site 2 (Fig. 12a) the VPR correction reduces the estimated accumulated rainfall close to the rain gauges measurement and the radar estimation from the PPI measurements at the elevation angle of 3°, which was below the melting layer and, thus, it was not affected by it. There is still an overestimation of the VPR corrected rainfall at the elevation angle of 4° with respect to the rain gauges during

the time period 1200–1300 UTC and an underestimation after 1300 UTC. However, similar but smaller differences from the rain gauges are observed in the lower-elevation angle.

The radar measurements at both elevation angles for site 5 (Fig. 12b) were in and above the melting layer. PPI scans were made also at lower-elevation angles (1° and 2°), but the radar beam was blocked by more than 40% in the direction of site 5. Thus, there was no elevation angle available without melting-layer effect for this site. The accumulated rainfall from the elevation angle of 3° is higher than the rain gauge measurements and the apparent VPR correction reduces it to values a little higher than rain gauges before 1200 UTC and a little lower at the end of the event, which is a similar trend as with the case of site 2. Considering the fact that site 5 is at a range larger than site 2 and that rain was approaching to the radar, this trend could be attributed mainly to the estimation error of the polarimetric algorithm. In the case of the elevation angle of 4° the radar estimation of accumulated rainfall at site 5 is much lower than rain gauge measurements, which is expected because the radar measurement altitude is in the snow region where the measured reflectivities and rainfall estimates are lower than their average values below the melting layer. Because of differential attenuation the differential reflectivity Z_{dr}, which typically presents a peak in the melting layer, gets negative values in the snow region (not shown here) despite the attenuation correction in the rain region below the melting layer. Thus, for the application of the polarimetric rainfall algorithm a theoretical positive Z_{dr} value has to be estimated from an average Z_h–Z_{dr} relation in rain (because the polarimetric algorithm does not accept negative Z_{dr} values), such as the relations presented by Bringi et al. (2001) and Park et al. (2005). However, this leads to an error in addition to the error due to the VPR. This is the reason that the accumulated rainfall estimate corrected for apparent VPR of rainfall estimate is still quite lower than rain gauge measurements. A solution to this problem, instead of using an average Z_h–Z_{dr} relation, is to correct first Z_{dr} for its vertical profile using the same approach as for reflectivity or rainfall estimation described in section 2b and then to correct the estimated rainfall for the remaining (mainly due to the VPR of Z_h and less for a possible systematic vertical profile of K_{dp}) effect of the melting layer. This method is noted as VPR–Z_{dr} in Fig. 12b and it gives a correction quite close to the rain gauge measurements. When this method is applied to measurement altitudes in the melting layer or in the snow region when the measured Z_{dr} does not get negative values the results are similar with the application of the single correction for the VPR of the rainfall estimate.

TABLE 1. NB and NSE statistics of accumulated rainfall estimation from the polarimetric algorithm presented in Figs. 9 and 12 separately for the cases of the measurement altitude h in or above the melting layer (h_b and h_t are the bottom and top boundaries, respectively, of the melting layer) and with and without correction for apparent VPR of rainfall estimate. In the VPR–Z_{dr} method, Z_{dr} has been corrected first for its apparent vertical profile before correcting for the vertical profile of rainfall estimate. The correlation coefficient for all cases is 0.99.

Position, VPR	NB (%)	NSE (%)
$h_b < h < h_t$, no VPR	27.3	35.1
$h_b < h < h_t$, VPR	0.4	13.7
$h > h_t$, no VPR	−39.5	55.3
$h > h_t$, VPR	−19.5	29.3
$h_t > h_t$, VPR–Z_{dr}	−0.5	12.2

Table 1 gives the error statistics for the accumulated rainfall estimated from the polarimetric algorithm with and without correction for apparent VPR using the data presented in Figs. 9 and 12. The normalized standard error (NSE) is the root-mean-square error normalized with respect to the mean reference value of the corresponding accumulated rainfall estimation, and normalized mean bias (NB) is the difference between the mean estimated and reference values normalized to the mean reference value. Reference values are the values from the disdrometer and the rain gauges measurements. The errors for the cases of the measurement altitude in the melting layer or above it in the snow region are given separately. The VPR–Z_{dr} method is the same as the one presented in Fig. 12b and described above. According to the statistical errors shown in this table, the correction for apparent VPR of rainfall estimate reduces significantly the bias and the standard error, which includes the bias and the random errors, because of melting-layer and snow region effects to values less than 1% and just above 10%, respectively. In the case of snow region, Z_{dr} has to be corrected first for its vertical profile to avoid cases with negative measured values, else a significant part (about half) of bias and standard errors remain.

4. Conclusions

A method to correct reflectivity measurements and rainfall estimates in PPI scans of polarimetric radars for apparent VPR was presented. The apparent VPR is proposed for application only to the scan from which it is estimated, and, thus, the estimation of the true VPR is not required. First, the boundaries of the melting layer are determined using the characteristic minimum of copolar correlation coefficient in the melting layer as proposed by Matrosov et al. (2007). The application of this method for melting-layer detection in PPI scans (especially the top boundary) was shown to be quite

more challenging than in RHI scans because of the use of slant profiles in PPI scans instead of vertical (interpolated) profiles in RHI scans. The most difficult case was the detection of melting layer in PPI scans at low-elevation angles and long ranges. Furthermore, it is noted that the copolar correlation coefficient thresholds, which are used in the detection scheme, have to be adjusted according to the performance of each radar system. Despite these limitations, the detection of melting layer with this polarimetric method was shown to be more robust than that based on the use of reflectivity measurements alone.

After detecting the melting-layer boundaries and correcting radar reflectivities for rain-path attenuation below the melting layer, the apparent VPR for a PPI scan was constructed by averaging the range profiles of reflectivity or rainfall estimate in all azimuth directions of the scan. The height of each profile was first scaled using the melting-layer boundaries that were detected for this profile to allow variations of the boundaries in the scan, whereas the reflectivity or rainfall estimate was normalized with respect to its value at the bottom of the melting layer. The assumption made in this approach was that the shape of the VPR does not change significantly in the time duration and the area of the scan. The reflectivity measurements, or rainfall estimates, were then corrected using the calculated apparent VPR.

The use of an apparent VPR for each PPI scan allows for real-time variations of the VPR shape and intensity in time and variations of the melting-layer boundaries in space and time. In addition this method can be used to correct for VPR PPI scans of any radar algorithm for rainfall estimation (including polarimetric algorithms) instead of correcting only reflectivity–rainfall algorithms. The detailed analysis of a 5-h rain event (28 March 2008) observed by the X-Pol radar showed that this method has better performance on average than using an idealized VPR profile, which requires a climatological tuning of its parameters. On average, based on results from that rain event and a daylong event (22 March 2007) with 90–150 mm (depending on location) accumulated rainfall the correction with apparent VPR was shown to remove most of the systematic error (less than 1% after correction) and decrease the standard error (just above 10% after correction) of rainfall estimates. In the melting layer the apparent VPR correction removed the circular-like zone of enhanced reflectivity or rainfall estimate. In the snow region, where the VPR predicts a high reduction of reflectivity or estimated rainfall rate, Z_{dr} has to be corrected first for its vertical profile to avoid the possible problem of negative values in the application of polarimetric algorithms.

In the snow region and at large ranges the correction removes the decrease of the observed VPR with range but may exhibit lower performance with an overestimation by 2 dB or more. This could be due to the decorrelation (probably at altitudes higher than 500 m above the melting-layer top based on the observations presented in Fig. 4) between the rainfall estimates at high altitudes with the rainfall field at the ground and the rapid decrease of reflectivity in the snow region. In addition, at long ranges beam broadening degrades significantly the polarimetric measurements. Kirstetter et al. (2010) noted that at 60–70-km range the degradation of radar measurements is too high and this is possibly the range limitation for stratiform VPR correction. When the radar altitude is above the bottom of the melting layer, the PPI at the lowest possible beam elevation angle does not sample below the melting layer and the method will not be applicable. This means, however, that RHI scans also will not include samples below the melting layer and, thus, neither RHI or a full volume scan can be used to construct a VPR profile. To estimate rainfall rate at ground level in mountainous areas the PPI with the minimum antenna elevation angle may be chosen so that the area of interest is not affected significantly by beam blockage or ground clutter by the terrain. This does not exclude the combination of PPI data from different elevation angles each corrected separately for VPR. Data to be collected in future experimental studies utilizing multiple disdrometers at various ranges from the radar will provide the basis to further validate the VPR correction method, and possible extensions to include a mixture of stratiform (rays where melting layer is detected) and convective type rain (rays where melting layer is not detected).

Acknowledgments. This work was supported in part by the HYDRORAD project (Research for SMEs category—Grand Agreement number FP7-SME-2008-1-232156) funded by EC 7th Framework Program from 2009 until 2011. Marios N. Anagnostou thanks the support of the Marie Curie Fellowship under the Grant Agreement Number 236871 HYDREX, coordinated by the Sapienza University of Rome, Italy and the support of the Postdoctoral Fellowship by the Greek General Secretariat for Research and Technology under the Grant Agreement Number PE10(975) HYDRO-X, coordinated by the National Observatory of Athens, Greece, in the framework of the program "Education and Lifelong Learning" funded by Greece and EU-European Social Fund.

REFERENCES

Anagnostou, M. N., J. Kalogiros, E. N. Anagnostou, and A. Papadopoulos, 2009: Experimental results on rainfall estimation in complex terrain with a mobile X-band polarimetric weather radar. *Atmos. Res.,* **94,** 579–595.

——, ——, ——, M. Tarolli, A. Papadopoulos, and M. Borga, 2010: Performance evaluation of high-resolution rainfall estimation by X-band dual-polarization radar for flash flood applications in mountainous basins. *J. Hydrol.,* **394,** 4–16.

——, ——, F. S. Marzano, E. N. Anagnostou, M. Montopoli, and E. Picciotti, 2013: Performance evaluation of a new dual-polarization microphysical algorithm based on long-term X-band radar and disdrometer observations. *J. Hydrometeor.,* **14,** 560–576.

Andrieu, H., and J. D. Creutin, 1995: Identification of vertical profiles of radar reflectivity for hydrological applications using an inverse method. Part I: Formulation. *J. Appl. Meteor.,* **34,** 225–239.

Battan, L. J., 1973: *Radar Observations of the Atmosphere.* University of Chicago Press, 279 pp.

Bellon, A., G. W. Lee, and I. Zawadzki, 2005: Error statistics of VPR corrections in stratiform precipitation. *J. Appl. Meteor.,* **44,** 998–1015.

Brandes, E. A., and K. Ikeda, 2004: Freezing-level estimation with polarimetric radar. *J. Appl. Meteor.,* **43,** 1541–1553.

Bringi, V. N., and V. Chandrasekar, 2001: *Polarimetric Doppler Weather Radar: Principles and Applications.* Cambridge University Press, 636 pp.

——, T. Keenan, and V. Chandrasekar, 2001: Correcting C-band radar reflectivity and differential reflectivity data for rain attenuation: A self-consistent method with constraints. *IEEE Trans. Geosci. Remote Sens.,* **39,** 1906–1915.

Delrieu, G., B. Boudevillain, J. Nicol, B. Chapon, P.-E. Kirstetter, H. Andrieu, and D. Faure, 2009: Bollène-2002 Experiment: Radar quantitative precipitation estimation in the Cévennes–Vivarais region, France. *J. Appl. Meteor. Climatol.,* **48,** 1422–1447.

Doviak, R. J., and D. S. Zrnić, 1993: *Doppler Radar and Weather Observations.* Academic Press, 562 pp.

Fabry, F., and I. Zawadzki, 1995: Long-term observations of the melting layer of precipitation and their interpretation. *J. Atmos. Sci.,* **52,** 838–851.

Gourley, J. J., and C. M. Calvert, 2003: Automated detection of the bright band using WSR-88D data. *Wea. Forecasting,* **18,** 585–598.

Harrold, T. W., and P. G. Kitchingman, 1975: Measurement of surface rainfall using radar when the beam intersects the melting layer. Preprints, *16th Conf. on Radar Meteorology,* Houston, TX, Amer. Meteor. Soc., 473–478.

Illingworth, A., and R. Thompson, 2011: Radar bright band correction using the linear depolarisation ratio. *Proc. Eighth Int. Symp. on Weather Radar and Hydrology,* Exeter, UK, IAHS Publ. 351, 64–68.

Kalogiros, J., M. N. Anagnostou, and E. N. Anagnostou, 2006: Rainfall retrieval from polarimetric X-band radar measurements. *Proc. Fourth European Conf. on Radar in Meteorology and Hydrology,* Barcelona, Spain, ERAD 2006, 145–148.

——, ——, ——, M. Montopoli, E. Picciotti, and F. S. Marzano, 2013a: Evaluation of a new polarimetric algorithm for rain path attenuation correction of X-band radar observations against disdrometer data. *IEEE Geosci. Trans. Remote Sens.,* doi:10.1109/TGRS.2013.2250979, in press.

——, ——, ——, ——, ——, and ——, 2013b: Optimum estimation of rain microphysical parameters from X-band dual-polarization radar observables. *IEEE Trans. Geosci. Remote Sens.,* **51,** 3063–3076.

Kirstetter, P.-E., H. Andrieu, G. Delrieu, and B. Boudevillain, 2010: Identification of vertical profiles of reflectivity for correction of volumetric radar data using rainfall classification. *J. Appl. Meteor. Climatol.,* **49,** 2167–2180.

Kitchen, M., 1997: Towards improved radar estimates of surface precipitation at long range. *Quart. J. Roy. Meteor. Soc.,* **123,** 145–163.

——, R. Brown, and A. G. Davies, 1994: Real-time correction of weather radar data for the effects of bright band, range and orographic growth in widespread precipitation. *Quart. J. Roy. Meteor. Soc.,* **120,** 1231–1254.

Marzano, F. S., E. Picciotti, and G. Vulpiani, 2004: Rain field and reflectivity vertical profile reconstruction from C-band radar volumetric data. *IEEE Trans. Geosci. Remote Sens.,* **42,** 1033–1046.

Matrosov, S. Y., K. A. Clark, and D. E. Kingsmill, 2007: A polarimetric radar approach to identify rain, melting layer, and snow regions for applying corrections to vertical profiles of reflectivity. *J. Appl. Meteor. Climatol.,* **46,** 154–166.

Mishchenko, M. I., 2000: Calculation of the amplitude matrix for a nonspherical particle in a fixed orientation. *Appl. Opt.,* **39,** 1026–1031.

Park, S., V. N. Bringi, V. Chandrasekar, M. Maki, and K. Iwanami, 2005: Correction of radar reflectivity and differential reflectivity for rain attenuation at X-band. Part I: Theoretical and empirical basis. *J. Atmos. Oceanic Technol.,* **22,** 1621–1632.

Rico-Ramirez, M. A., and I. D. Cluckie, 2007: Bright-band detection from radar vertical reflectivity profiles. *Int. J. Remote Sens.,* **28,** 4013–4025.

——, ——, and D. Han, 2005: Correction of the bright band using dual-polarisation radar. *Atmos. Sci. Lett.,* **6,** 40–46.

Ryzhkov, A., 2007: The impact of beam broadening on the quality of radar polarimetric data. *J. Atmos. Oceanic Technol.,* **24,** 729–744.

Smith, C. J., 1986: The reduction of errors caused by bright bands in quantitative rainfall measurements using radar. *J. Atmos. Oceanic Technol.,* **3,** 129–141.

Smyth, T. J., and A. J. Illingworth, 1998: Radar estimates of rainfall rates at the ground in bright band and non-bright band events. *Quart. J. Roy. Meteor. Soc.,* **124,** 2417–2434.

Vignal, B., H. Andrieu, and J. D. Creutin, 1999: Identification of vertical profiles of reflectivity from volume scan radar data. *J. Appl. Meteor.,* **38,** 1214–1228.